Optics Communications 284 (2011) 5556–5561

Contents lists available at SciVerse ScienceDirect

Optics Communications

journal homepage: www.elsevier.com/locate/optcom

Restoration of atmospheric turbulence degraded images

Dongfeng Shi, Chengyu Fan *, Hong Shen, Pengfei Zhang, Chunhong Qiao, Xiaoxing Feng, Yingjian Wang

Key Laboratory of Atmospheric Composition and Optical Radiation, Anhui Institute of Optics and Fine Mechanics, Chinese Academy of Sciences, Hefei 230031, China

ARTICLE INFO

Article history:
Received 19 May 2011
Received in revised form 28 July 2011
Accepted 1 August 2011
Available online 31 August 2011

Keywords:
Blind multiframe deconvolution
Atmospheric turbulence
Regularization

ABSTRACT

A blind image deconvolution algorithm in the frequency domain is proposed which uses the edge-preserving method and generic bandwidth of optical system. Generic bandwidth of optical system is analyzed. With the benefits of bandwidth and edge-preserving method as compelling constraints, the algorithm cannot only suppress noise effectively but also restrict the bandwidth of point-spread function (PSF), so high-quality result can be obtained. The new algorithm is superior in handling unregistered channels. The performance of this approach is investigated with simulated data. As shown in our investigation, the algorithm can significantly alleviate the artifacts produced by the deconvolution process.

1. Introduction

The performance of high-resolution imaging with ground-based telescope is severely limited by atmospheric turbulence. A number of methods have been proposed to obtain high resolution images [1]. Speckle imaging [2–4] relying on post detection computer processing of large numbers of the short exposure images is the first attempt to overcome the effects of turbulence. Adaptive optics [5–7], another crucial technique, can only partly overcome the limitation of atmospheric turbulence because of measurement error. In addition, it is expensive to build and maintain adaptive optics systems. Blind deconvolution [8–29] is an important post-processing technique in which the complete knowledge of both the point spread function (PSF) and the original image is not available. The aim of blind deconvolution is to gain an estimate of the original high-resolution image based on the blurred observations.

One of the most widely used blind deconvolution is the multiframe blind deconvolution (MBD) [14–29] which is applied to sequences of images of a target obtained over time scales such that the target can be considered stationary but the PSFs are changing. It is common for the objects observation through the atmosphere. In general, the fidelity and resolution of the restoration is directly related to the amount and quality of prior information employed to constrain the resolution. At present, almost all of the MBD algorithms use the constraints of non-negativity, finite support and normalization. With regard to the PSFs estimation generated in iteration, the frequency is variable. Considered the optical imaging system, the frequency spectrum of a PSF turns zero when it is beyond the cutoff frequency in blind deconvolution [16]. The relationship between the parameters of the telescope's optical system and the bandwidth constraint in the pixel spatial domain is reported [17], but it is only applied in special situation where the CCD is square. In this paper, the bandwidth of generic situation is analyzed and applied as constraint in the blind deconvolution problem. Because the approach in this article is implemented in the frequency domain, the bandwidth constraint can be directly employed. The image, gotten from iteration, is stained by noise. However, the nonuniqueness and sensitivity of the solution to noise are still serious problems. Some measures have been taken to suppress noise as reported [8,19], but details of image are blurred at the same time. In order to solve this problem, an eximious method [30] is used for image denoising in iteration, which can effectively preserve the details of image. Even so, the image is still slightly blurred. So the principal objective of sharpening spatial filters [31] is introduced to enhance the details that have been blurred. Using image sharpening after image denoising can overcome this shortcoming.

The space object identification involves tracking and imaging from ground-based telescopes in attempt to identify and catalog the objects. But the object cannot be accurately tracked by a telescope. As a result, the position of the same object in the images obtained at different time will shift. In this situation, two stages are contained in image restoration: image registration which brings the channels into spatial alignment; multichannel blind deconvolution. Hundreds of image registration methods have been published, such as [32,33], but perfect registration accuracy can rarely be achieved. The registration error results in a slight shift of up to a few pixels between-channels and the channel misregistrations would lead to strong artifacts in the restored image [20]. Alternating minimization maximum a posterior (AMMAP) [20] is the first method explicitly dealing with unregistration of the images in the multichannel framework. In this paper, our method provides a successful solution to this problem.

The rest of this paper is arranged as follows. Section 2 provides an overview of the multiframe blind deconvolution. In Section 3, generic

* Corresponding author.
E-mail address: cyfan@aiofm.ac.cn (C. Fan).

0030-4018/$ – see front matter © 2011 Elsevier B.V. All rights reserved.
doi:10.1016/j.optcom.2011.08.039

bandwidth of optical imaging system and edge-preserving method are explained. In Section 4, we apply the image reconstruction technique to reconstructing the simulated images, and conclusions are given in Section 5.

2. Multiframe blind deconvolution

Within the isoplanatic angle, the short-exposure image $g_j(x,y)$ at the focal plane of the optical imaging system considering the effect of atmosphere is given by

$$g_j(x,y) = \left(h^j_{atm} * h_{opt} * f\right)(x,y) + n_j(x,y), \quad j = 1,\ldots,M, \tag{1}$$

where $g_j(x,y)$, $f(x,y)$ and $n_j(x,y)$ represent the observed images, the original image and the observation noise, respectively, M is the number of the frames, and j refers to the j-th data frame. The images are blurred by both the atmospheric turbulence and the optical imaging system represented by the point spread functions $h^j_{atm}(x,y)$ and $h_{opt}(x,y)$, respectively. The operator $(*)$ denotes two-dimensional convolution. In this paper, $h_j(x,y) = (h^j_{atm} * h_{opt})(x,y)$ is introduced. First, consider the least squares likelihood function:

$$E_{data}(f,h) = \sum_{j=1}^{M} \left\| g_j(x,y) - \left(h_j * f\right)(x,y) \right\|^2 \tag{2}$$

Here, $\|\cdot\|$ denotes the standard L^2 norm and $h = (h_1,\ldots,h_M)$. As the blind deconvolution is an ill-posed problem, we add regularization terms. Thikhonov regularization is used, and Eq. (2) is replaced by

$$E(f,h) = \sum_{j=1}^{M} \left\| g_j(x,y) - \left(h_j * f\right)(x,y) \right\|^2 + \gamma_1 \|f(x,y)\|^2 + \gamma_2 \sum_{j=1}^{M} \left\| h_j(x,y) \right\|^2 \tag{3}$$

Here, γ_1 and γ_2 are the positive regularization parameters. According to the convolution theorem and the fact that Fourier transforms [34] preserve L^2 norm, we can express Eq. (3) in terms of Fourier transforms:

$$E(F,H) = \sum_{j=1}^{M} \left\| G_j(u,v) - \left(H_j F\right)(u,v) \right\|^2 + \gamma_1 \|F(u,v)\|^2 + \gamma_2 \sum_{j=1}^{M} \left\| H_j(u,v) \right\|^2 \tag{4}$$

Here, $G_j(u,v) = \mathbf{F}\{g_j(x,y)\}$, $H_j(u,v) = \mathbf{F}\{h_j(x,y)\}$, $F(u,v) = \mathbf{F}\{f(x,y)\}$, $\boldsymbol{H} = \mathbf{F}\{\boldsymbol{h}\}$ and $\mathbf{F}$ denotes the 2-D Fourier transform. The u,v are the coordinates in the frequency domain.

An alternating minimization method is applied to obtain a minimizer of the objective function $E(F,H)$. For any starting values $F^{(0)}$ and $H^{(0)}$, the values $F^{(n+1)}$ and $H^{(n+1)}$ can be procured through approaching cycle between the image and PSFs estimation steps. In the image estimation step the image $F^{(n+1)}$ is estimated assuming that the PSFs are fixed to $\widehat{H}^{(n)}$ which are the latest estimate from the PSFs estimation step and subjected to the bandwidth constraint, and the image is fixed to $\widehat{F}^{(n)}$ which is the latest estimate from the image estimation step and processed by the edge-preserving method. The bandwidth constraint and the edge-preserving method will be introduced in the next section. The image estimation step uses the following equation:

$$F^{(n+1)} = \widehat{F}^{(n)} - \alpha \partial_{F^*} E\left(\widehat{F}^{(n)}, \widehat{H}^{(n)}\right) \Big/ \partial_F \partial_{F^*} E.$$

$$\Longleftrightarrow F^{(n+1)} = (1-\alpha)\widehat{F}^{(n)} + \alpha \sum_{j=1}^{M} G_j \widehat{H}_j^{*(n)} \Bigg/ \left(\sum_{j=1}^{M} \left| \widehat{H}_j^{*(n)} \right|^2 + \gamma_1 \right).$$

In the PSFs estimation step the PSFs $H^{(n+1)}$ are estimated assuming that the image is fixed to $\widehat{F}^{(n+1)}$ which is estimated from the above image estimation step and processed by the edge-preserving method. The estimated value $H^{(n+1)}$ can be achieved by the following equation:

$$H_j^{(n+1)} = \widehat{H}_j^{(n)} - \beta \partial_{\widehat{H}_j^*} E\left(\widehat{F}^{(n+1)}, \widehat{H}_j^{(n)}\right) \Big/ \partial_{\widehat{H}_j} \partial_{\widehat{H}_j^*} E.$$

$$\Longleftrightarrow H_j^{(n+1)} = (1-\beta)\widehat{H}_j^{(n)} + \beta G_j \widehat{F}^{(n+1)} \Big/ \left(\left| \widehat{F}^{(n+1)} \right|^2 + \gamma_2 \right), j = 1,\ldots,M.$$

Here, the parameters α, β are the step sizes in the recursions. The constraints of non-negativity, finite support and normalization are effective and widely used. Thinking over the optical imaging system, the bandwidth of optical imaging system is limited. The PSFs in frequency domain acquired from the step of iteration are variable, and the values which exceed the cutoff frequency of optical transfer function (OTF) are invalid. For the sake of solving this problem, constraint of bandwidth is employed [16]. The authors [17] have referred the relationship between the parameters of optical imaging system in special situation where the CCD is square and the bandwidth constraint in pixel spatial domain. Here, bandwidth of generic optical imaging system is analyzed and introduced as the constraint in the blind deconvolution. The image from iteration is stained by noise. Inasmuch as the nonuniqueness and the sensitivity of the solution to the noise are still serious problems, measures are needed to be taken to restrain noise. The edge-preserving method cannot only suppress noise effectively but also preserve the details of the image.

3. Generic bandwidth of optical imaging system and edge-preserving method

3.1. Generic bandwidth of optical imaging system

The bandwidth of the PSFs in the frequency domain is variable, and possibly exceeds the cutoff frequency of optical transfer function (OTF) so it produces the trivial estimation. To overcome the disadvantage, generic bandwidth of optical imaging system is obtained, which can prevent the bandwidth of the PSFs from exceeding the cutoff frequency of the OTF. Suppose the size of CCD is $N_x \times N_y$. We will analyze the generic situation where N_x is not equal to N_y. If the size of pixel is N_p, the number of pixels along the diameter of Airy disk for an ideal optical system is

$$N_A = \left(\frac{2.44\lambda l}{D}\right)\frac{1}{N_p},$$

where λ,D and l are the wavelength, the aperture diameter and the distance from the exit pupil to the imaging plane, respectively.

The frequency of the diameter of Airy disk can be expressed as $1/N_A$ and considered as the cutoff frequency. According to Fourier optical theory [34], the bandwidth of the OTF is twice the cutoff frequency. In order to obtain the bandwidth constraint, we have to make sure that the diffraction spots, which are produced by the optical system and the effective aperture pupil in the frequency domain, have the same size. According to this relationship, the effective aperture pupil of generic optical imaging system is

$$P(u,v) = \begin{cases} 1, & (2(u-u_0)/N_{cx})^2 + \left(2(v-v_0)/N_{cy}\right)^2 \le 1 \\ 0, & (2(u-u_0)/N_{cx})^2 + \left(2(v-v_0)/N_{cy}\right)^2 > 1 \end{cases},$$

where $u_0 = N_x/2, v_0 = N_y/2$, N_{cx} and N_{cy} are the number of pixels of bandwidth in the u direction and v direction, respectively, defined by

$$N_{cx} = 2N_x/N_A = \left(\frac{D}{1.22\lambda l}\right)N_p N_x,\ N_{cy} = 2N_y/N_A = \left(\frac{D}{1.22\lambda l}\right)N_p N_y.$$

The bandwidth of the estimated PSFs at every iteration should be constrained to avoid the trivial estimation, which can be expressed as

$$\widehat{H}_j^{(n)} = H_j^{(n)} P(u,v),$$

where $H_j^{(n)}$ is the estimate from the PSFs estimation step in the n-th iteration. In the next iteration, the value $\widehat{H}_j^{(n)}$ is employed. If $N_x = N_y$, $P(u,v)$ will become the constraint in special situation where the size of CCD is square [17].

3.2. Edge-preserving method

In addition, the image from iteration is stained by noise. Because the solution of the MBD is sensitive to the noise, the quality of the result may be poor. In order to solve the problem, measures are needed to be taken to restrain noise. General filters can be used to suppress noise, but details of image are blurred at the same time. In this paper, we utilize the data-adaptive filters to filter the image for denoising. Data-adaptive filter [30] is an effective tool for denoising. It can preserve details and reduce noise effect in high SNR case. By defining $K_l(x_i - x)$, $x_i = [x_i, y_i]^T, x = [x, y]^T$ as the data-adaptive kernel function, $z(x)$ as the true pixel value which we wish to reconstruct at the position x, and $f_i^{(n)}$ the recovered image from the image estimation step in the n-th iteration in the spatial domain as the *ith* sample at the position x_i within a local neighborhood of which the center is x, we can express $z(x)$ as

$$z(x) = \sum_i K_l\,(x_i - x) f_i^{(n)} / \sum_i K_l(x_i - x),$$

where the $K_l(x_i - x)$ can be written as

$$K_l(x_i - x) = \frac{\sqrt{\det(C_i)}}{2\pi h^2} \exp\left\{ -\frac{(x_i - x)^T C_i (x_i - x)}{2h^2} \right\},$$

where h is the global smoothing parameter and C_i is the covariance matrix [30] which can be expressed as

$$C_i = \gamma_i U_{\theta_i} \Lambda_i U_{\theta_i}^T,$$

$$U_{\theta_i} = \begin{bmatrix} \cos\theta_i & \sin\theta_i \\ -\sin\theta_i & \cos\theta_i \end{bmatrix}, \Lambda_i = \begin{bmatrix} \sigma_i & 0 \\ 0 & \sigma_i^{-1} \end{bmatrix},$$

where U_{θ_i} is the rotation matrix and Λ_i is the elongation matrix. The parameters γ_i, θ_i and σ_i are the scaling, rotation, and elongation parameter, respectively. The details of estimating these parameters are described as follow.

$$G = \begin{bmatrix} \vdots & \vdots \\ f_{i,x}^{(n)} & f_{i,y}^{(n)} \\ \vdots & \vdots \end{bmatrix} = U_i S_i V_i^T,$$

where $f_{i,x}^{(n)}$ and $f_{i,y}^{(n)}$ are the first derivatives along x and y directions. The second column of the 2×2 orthogonal matrix V_i, $v_2 = [v_1, v_2]^T$, defines the dominant orientation angle θ_i

$$\theta_i = \arctan\left(\frac{v_1}{v_2}\right).$$

The diagonal 2×2 matrix S_i represents the energy in the dominant directions. The elongation parameter σ_i and the scaling parameter γ_i can be defined by

$$\sigma_i = \frac{s_1 + \lambda'}{s_2 + \lambda'}, \gamma_i = \left(\frac{s_1 s_2 + \lambda''}{M} \right)^{1/2},$$

where λ' and λ'' are the regularization parameters, and M is the number of samples. Similar to the paper [30], $\lambda' = 1.0$ and $\lambda'' = 0.01$ are chosen.

This method can preserve edge, but slightly blurs it. Moreover Thikhonov regularization in Eq. (3) often yields results that are oversmoothed and compromises image contrast when applied uniformly to all object features. To solve this problem, image sharpening [31] is employed which can be defined as

$$\widehat{f}^{(n)} = z(x) - \kappa z_{lp}(x),$$

here, the image $z_{lp}(x)$ is acquired by filtering $z(x)$ using the Laplacian filter and κ is the tuning parameter. The Laplacian filter adopted can be described as

$$L = [\ 1\ \ 1\ \ 1\ \ ;\ \ 1\ \ -8\ \ 1\ \ ;\ \ 1\ \ 1\ \ 1\ ].$$

Edge-preserving method includes two parts: $z(x)$ is obtained by the data-adaptive filters to filter the recovered image $f^{(n)}$, and then image sharpening is employed to enhance the details of $z(x)$. In the next iteration, the value $\widehat{F}^{(n)}$ is employed which is the Fourier transform of the $\widehat{f}^{(n)}$.

4. Numerical examples

In this section we describe some numerical experiments to illustrate the potential advantages of the approach proposed in this paper. Random phase screens are generated according to the Kolmogorov spectrum [1]. These images, which are presented by 320×240 pixel array, represent the short-exposure turbulence degraded images recorded by a 1-m telescope with the atmospheric seeing parameter r_0, the nominal wavelength $\lambda = 650$ nm, $l = 20$ m, and $N_p = 6.5$ μm. According to these parameters, we can get $N_{cx} = 131.15$, $N_{cy} = 98.36$. The regularization parameters γ_1, γ_2 actually hardly influence the results and they are taken as 10^{-4}. The step sizes in the recursions are fixed to $\alpha = 0.8, \beta = 0.6$ which give good quality of the reconstructed images in a variety of scenarios. We introduce root mean square error (RMSE) as the recovered image quality evaluation criterion. The equation is expressed as follows: $RMSE = \sqrt{\sum (f_t - f_r)^2 / N}$, where f_t is the true image, f_r is the restored image and N is the number of samples in $f_r f_t$. In all experiments, the parameters for the edge-preserving method are manually optimized to produce the best RMSE values.

In the experiment, the image "Satellite" Fig. 1(A) is employed. The image is blurred at atmospheric seeing parameter $r_0 = 10$ cm and then white Gaussian noise (SNR = 50 dB) is added. Fig. 1(B) is one of the three blurred and noisy images which are the input images in algorithms. The support size of PSF is 35 pixels. The multichannel alternating minimization (MCAM) [18] introduces total variation (TV), and the result Fig. 1(C) after 300 iterations appears many artifacts, such as noise and ringing, inside the shapes and near their edges. Our method produces relatively high-quality result Fig. 1(D) with $h = 1, \kappa = 0.05$after 120 iterations. Via the bandwidth constraint of the PSF and with edge-preserving method to restrain noise in our algorithm, the ringing and noise artifacts are well suppressed in Fig. 1(D) compared to Fig. 1(C). Fig. 1(C) is a result with ringing and noise artifacts. However, more details are restored in Fig. 1(D). The RMSE values of the images of Fig. 1(C–D) are 18.54, and 9.59, respectively. Similarly, we manually change the parameters of MCAM to find the restored images with best RMSE value. Moreover, it could take about two days for the MCAM method to reach 300 iterations, but our method reached 120 iterations using about thirty minutes (CPU E5300 2.60 GHz, 2 G EMS memory using MatLab 7.0.4).

Next, we modify the previous experiment by atmospheric turbulence $r_0 = 13$ cm and adding white Gaussian noise SNR = 40 dB. One of the three resulting images is shown in Fig. 2(B) which is one of the input images in algorithms. The support size of PSF is 29 pixels. The

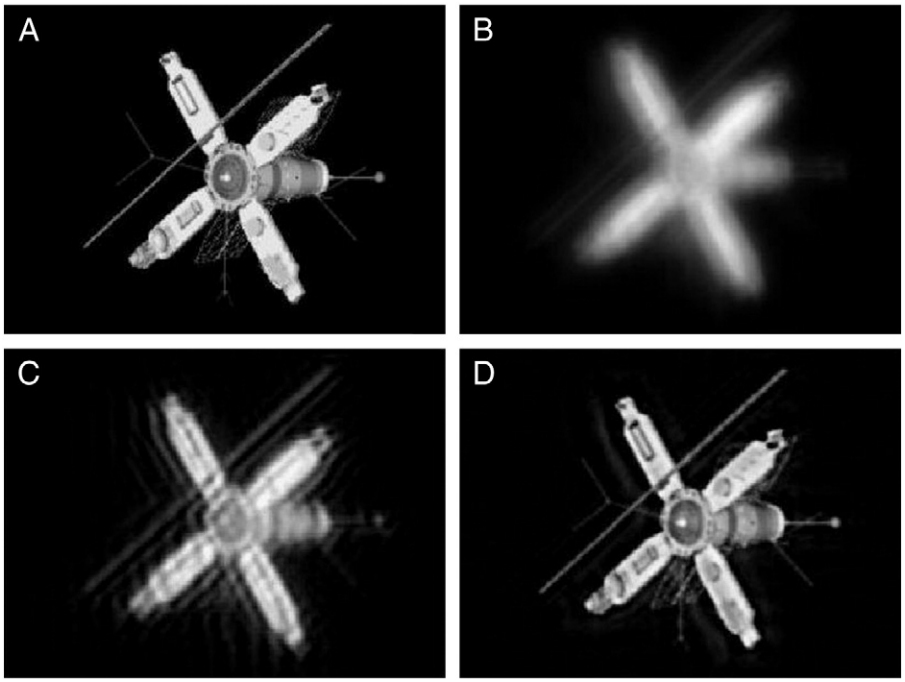

Fig. 1. Restorations of the simulated astronomy images ($r_0 = 10$ cm): (A) original image, (B) one of the three blurred and noisy images, (C) image restored with MCAM, and (D) image restored with our approach.

results of applying MCAM [18] with TV (200 iterations), and our approach ($h = 0.9$, $\kappa = 0.01$ after 50 iterations) are given in Fig. 2 (C) and (D), respectively. Fig. 2(C) is a result with noise artifacts. The noise artifacts are well suppressed in Fig. 2(D). Relatively high-quality result can be obtained through our method as seen from comparing Fig. 2(D) with Fig. 2(C). The corresponding RMSE values are 15.23(C), and 6.97(D). For the sake of comparison, a line plot is made to demonstrate the improvement in contrast and resolution. This is shown in Fig. 3 and it can be also found that Fig. 2(D) is of high resolution. In this experiment, the MCAM method takes about four hours to reach 200 iterations, and our method reached 50 iterations using about seven minutes. We note that execution time of MCAM method is influenced seriously by the support size of the PSF. When the support size of the PSF is big, execution time of MCAM method will be very long. However, execution time of our method hardly influenced by the support size of the PSF. Our method will become an efficient online scheme that models the multiframe problem more realistically through using the accelerated method [26].

Another advantage of the new algorithm is the ability to handle channels which are not registered. We will illustrate it in the subsequent

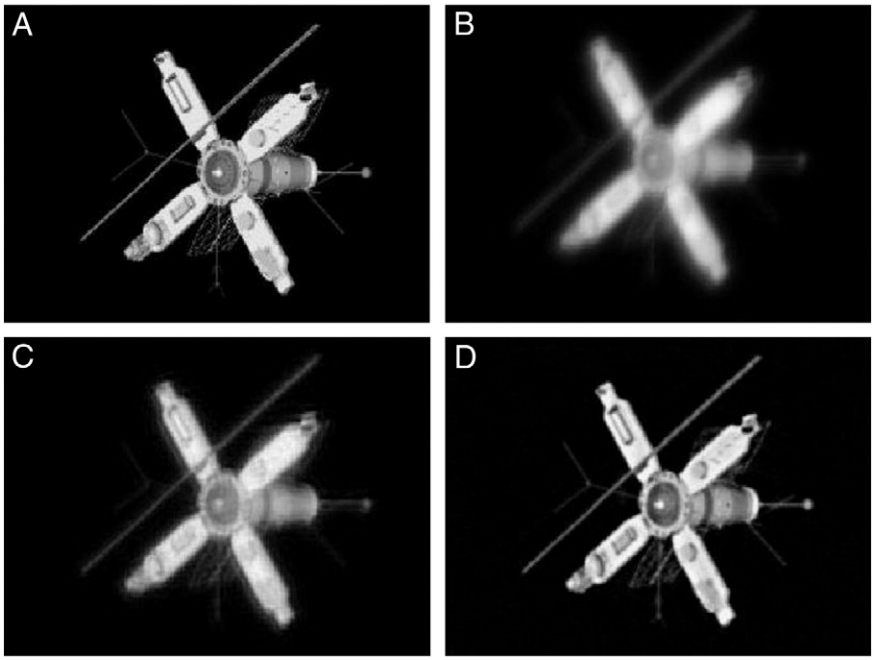

Fig. 2. Restorations of the simulated astronomy images ($r_0 = 13$ cm): (A) original image, (B) one of the three blurred and noisy images, (C) image restored with MCAM, and (D) image restored with our approach.

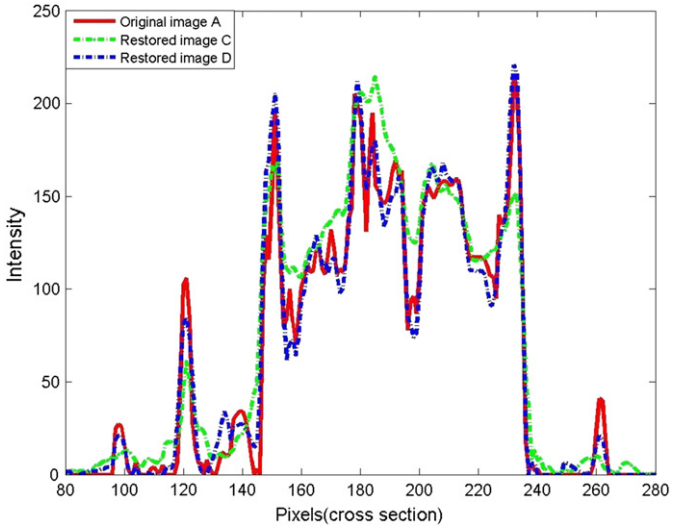

Fig. 3. This is a line plot taken across the horizontal axis of original image, Image restored with MCAM, Image restored with our approach.

experiment. The image "Satellite" is degraded with the same PSFs ($r_0 = 13$cm) and noise of SNR = 50 dB. The second and the third blurred images are shifted by [8 5] and [−3–8] pixels, respectively, as shown

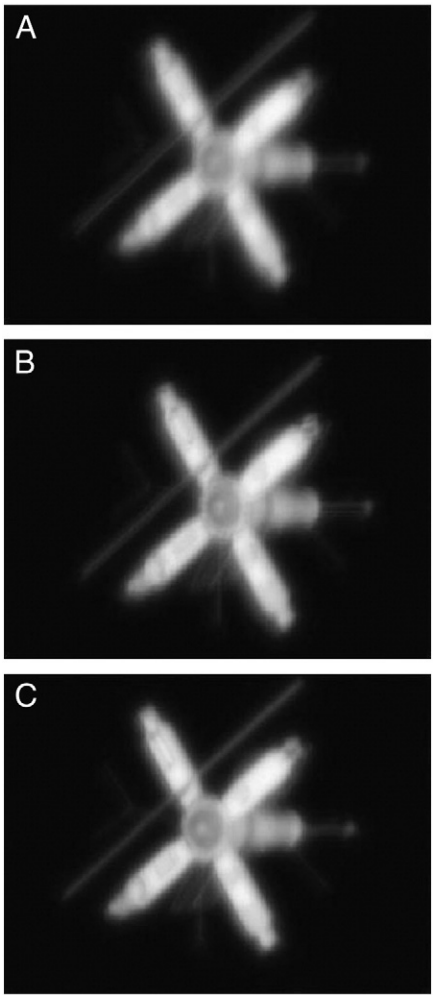

Fig. 4. Unregistered blurred noisy images: (A) first channel (B) second channel (shifted by [8 5] pixels), and (C) third channel (shifted by [-3 -8] pixels).

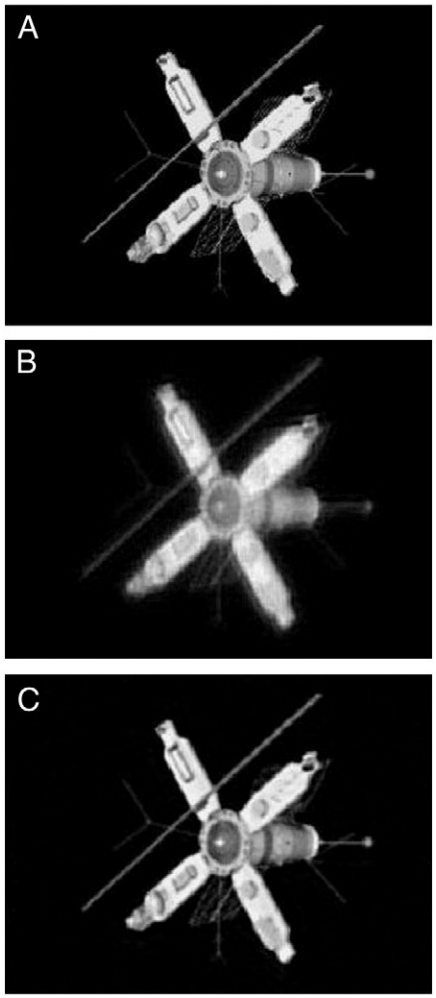

Fig. 5. (A) Original image, (B) image restored with MCAM, (C) recovered image from channel unregistered.

in Fig. 4. The support size of PSF is 37 pixels. The results of applying AM-MAP [20] with TV (500 iterations), and our approach ($h = 0.9$, $\kappa = 0.01$ after 150 iterations) are shown in Fig. 5(B–C), respectively, with RMSE values of (B) 15.29 and (C) 8.36. Our method resulted in an image with a better RMSE value. Comparing Fig. 5(B) with Fig. 5 (C), it can be found that the noise artifacts on the surface of the Satellite are apparently reduced and sharper edge is shown in Fig. 5(C). In this experiment, the AM-MAP method to reach 500 iterations takes about four days, and our method reached 150 iterations using about twenty minutes. Although the images are unregistered, the high-quality result can be obtained. Again, we also manually change the parameters of AM-MAP to find the restored images with best RMSE value.

5. Conclusions

A blind image deconvolution algorithm in the frequency domain is presented which uses the edge-preserving method and generic bandwidth of optical system. Data-adaptive filters are employed for image denoising and then sharpening spatial filters are adopted to highlight fine details in the image. Considering the restriction of the optical system diffraction limit, constrain of limited frequency-domain bandwidth is applied to the blind deconvolution. The quality of images restored by the proposed algorithm is higher. It possesses the predominance in the wide application of the real astronomical image, because the observed images misalignment occurs very frequently and the point spread functions are unknown.

Acknowledgments

The authors are indebted to the anonymous referees for their instructive comments and suggestions. This work is supported by Hefei Institutes of Physical Sciences, Chinese Academy of Sciences (grant nos. 073RC11123 and XJJ-11-S106).

References

[1] M.C. Roggemann, Imaging Through Turbulence, CRC Press, Boca Raton, 1995.
[2] A.W. Lohmann, G. Weigelt, B. Wirnitzer, Applied Optics 22 (1983) 4028.
[3] G.R. Ayers, M.J. Northcott, J.C. Dainty, Journal of the Optical Society of America. A 5 (1988) 963.
[4] M.C. Roggemann, E.L. Caudill, D.W. Tyler, M.J. Fox, M.A.V. Bokern, C.L. Matson, Applied Optics 33 (1994) 3099.
[5] M.C. Roggemann, B.M. Welsh, Applied Optics 33 (1994) 5400.
[6] J. Primot, G. Rousset, J.C. Fontanella, Journal of the Optical Society of America. A 7 (1990) 1598.
[7] L.A. Thompson, Physics Today 47 (12) (1994) 24.
[8] G.R. Ayers, J.C. Dainty, Optics Letters 13 (1988) 547.
[9] J.N. Caron, N.M. Namazi, R.L. Lucke, C.J. Rollins, J.P.R. Lynn, Optics Letters 26 (2001) 1164.
[10] Z. Xu, E.Y. Lam, Optics Letters 34 (2009) 1453.
[11] J. Bardsley, S. Jefferies, J. Nagy, R. Plemmons, Optics Express 14 (2006) 1767.
[12] G. Desiderà, M. Carbillet, Astronomy and Astrophysics 507 (3) (2009) 1759.
[13] H. Liao, M.K. Ng, IEEE Transactions on Image Processing 20 (2011) 670.
[14] D.A. LeMaster, S.C. Cain, Journal of the Optical Society of America. A 25 (2008) 2170.
[15] T.J. Schulz, Journal of the Optical Society of America. A 10 (1993) 1064.
[16] N. Miura, Optics Letters 28 (2003) 2312.
[17] Z. Hao, L. Yu, W. Qinzhang, Optics Letters 32 (2007) 2550.
[18] F. Sroubek, J. Flusser, IEEE Transactions on Image Processing 12 (2003) 1094.
[19] V. Katkovnik, J. Astola, Blind Image Deconvolution, CRC Press, 2009.
[20] F. Sroubek, J. Flusser, IEEE Transactions on Image Processing 14 (2005) 874.
[21] S.V. Vorontsov, V.N. Strakhov, et al., Optics Express 19 (14) (2011) 13509.
[22] M. Hirsch, S. Harmeling, et al., Astronomy and Astrophysics 531 (2011) A9.
[23] T. Schulz, B. Stribling, J. Miller, Optics Express 1 (1997) 355.
[24] S.M. Jefferies, M. Hart, Optics Express 19 (3) (2011) 1975.
[25] J. Zhang, Q. Zhang, et al., Applied Optics 48 (12) (2009) 2350.
[26] Y.-W. Wen, C. Liu, et al., Applied Optics 49 (15) (2010) 2761.
[27] J. Zhang, Q. Zhang, G. He, Optics Letters 33 (2008) 25.
[28] W. Souidene, K. Abed-Meraim, A. Beghdadi, IEEE Transactions on Image Processing 18 (2009) 1487.
[29] M.S. Almeida, L.B. Almeida, IEEE Transactions on Image Processing 19 (2010) 36.
[30] H. Takeda, S. Farsiu, P. Milanfar, IEEE Transactions on Image Processing 16 (2007) 349.
[31] R. Gonzalez, R. Woods, Digital Image Processing, Addison-Wesley Longman Publishing Co., Inc, 2001.
[32] M. Guizar-Sicairos, S.T. Thurman, J.R. Fienup, Optics Letters 33 (2008) 156.
[33] Z.-l. Song, S. Li, T.F. George, Optics Express 18 (2010) 513.
[34] J.W. Goodman, Introduction to Fourier Optics, McGraw-Hill, 1996.